J. Fluid Mech. (2010), *vol.* 645, *pp.* 435–446.
doi:10.1017/S0022112009993132

A numerical study of global frequency selection in the time-mean wake of a circular cylinder

J. S. LEONTINI[1,2]†, M. C. THOMPSON[1,2] AND K. HOURIGAN[1,2]

[1]Fluids Laboratory for Aeronautical and Industrial Research (FLAIR), Department of Mechanical Engineering, Monash University, Melbourne, Victoria 3800, Australia

[2]Division of Biological Engineering, Monash University, Melbourne, Victoria 3800, Australia

(Received 30 July 2009; revised 30 October 2009; accepted 30 October 2009; first published online 4 February 2010)

A series of direct numerical simulations, both in two- and three-dimensions, of the flow past a circular cylinder for Reynolds numbers $Re \leqslant 600$ has been conducted. From these simulations, the time-mean (and, for the three-dimensional simulations, the spanwise spatial-mean) flow has been calculated. A global linear stability analysis has been conducted on these mean flows, showing that the mean cylinder wake for $Re \leqslant 600$ is marginally stable and the eigenfrequency of the leading global mode closely predicts the eventual saturated vortex shedding frequency. A local stability analysis has also been conducted. For this, a series of streamwise velocity profiles has been extracted from the mean wake and the stability of these profiles has been analysed using the Rayleigh stability equation. The real and imaginary instability frequencies gained from these profiles have then been used to find the global frequency selected by the flow using a saddle-point criterion. The results confirm the success of the saddle-point criterion when the mean flow is quasi-parallel in the vicinity of the saddle point; however, the limitations of the method when the mean flow exhibits higher curvature are also elucidated.

1. Introduction

The periodic vortex shedding into the wake of a circular cylinder is one of the most well-known examples of a global fluid instability in an open flow. Over a wide range of Reynolds numbers, the flow selects a single frequency and is essentially unaffected by small disturbances upstream. This makes it an example of a global absolute instability (Huerre & Monkewitz 1985), when it is studied in the context of an open shear flow.

There is a large body of work treating the cylinder wake as a slowly varying, parallel shear flow (see the review of Chomaz 2005 and references therein). To facilitate this, either the steady solution is studied or the mean of the time-periodic wake is investigated. Recent studies have had success studying the mean flow, employing a saddle-point criterion to find the frequency of the global mode growing on the mean. These studies have concentrated on the two-dimensional flow (where $Re < 190$), either experimentally (Khor, Sheridan & Hourigan 2008*a*) or numerically.

The global stability of the mean flow has also been studied directly (Barkley 2006), showing that the mean is marginally stable when the flow is two-dimensional. In that paper, it was highlighted that analysing the mean flow in this way assumes that the

† Email address for correspondence: justin.leontini@eng.monash.edu.au

Reynolds stresses induced by the fluctuating wake are unperturbed at linear order. The asymptotic analysis of Sipp & Lebedev (2007) showed that, for the cylinder wake, the flow can be well represented by a mean and a single mode, with little nonlinear interaction between them, hence validating the assumption that the Reynolds stresses are unperturbed. Sipp & Lebedev (2007) concluded that this is not necessarily true of all periodic flows. It should be noted, however, that their analysis was strictly valid only very close to the bifurcation point and does not completely explain the success of the global analysis of Barkley (2006) over a wide range of Reynolds number.

It is therefore natural to enquire as to whether these analysis techniques can be extended to situations where the flow is three-dimensional. This paper studies this question. First, the two-dimensional flow is studied at Reynolds numbers both above and below the natural transition to three-dimensionality, using both the locally based saddle-point criterion and a full global stability analysis. The fully three-dimensional flow is then studied by employing direct numerical simulations (DNSs) to obtain the mean wake flows.

It is shown that the saddle-point criterion works very well, even when the flow is three-dimensional, provided the local curvature is not too high, and the assumption that the flow is slowly varying is reasonable. The global analysis shows that the spanwise-averaged mean wake remains marginally stable even for the three-dimensional flow, supporting the hypothesis that the cylinder wake dynamics are dominated by the first linear mode growing on a nonlinear corrected mean flow.

2. Methodology and validation

2.1. *Computational prediction*

The time-dependent velocity field was predicted using a spectral-element code validated extensively from previous studies of related flows (Thompson, Hourigan & Sheridan 1996; Thompson, Leweke & Williamson 2001; Ryan, Thompson & Hourigan 2005; Leontini, Thompson & Hourigan 2007). The code employs a spectral-element method for the spatial differencing in a plane and a Fourier decomposition for the spatial differencing in the spanwise direction. The mesh used had a blockage ratio of 3.3 %, with the upstream and side boundaries placed $15D$ from the centre of the cylinder. The outflow boundary was positioned $30D$ downstream from the cylinder. For the three-dimensional simulations, a spanwise extent of $16D$ was used. Either 96 or 128 Fourier planes were used, depending on the Reynolds number. The mesh was concentrated towards the cylinder boundary to properly resolve the boundary and separating shear layers. The resolution could be adjusted at runtime by changing the order of the tensor-product Lagrangian interpolating polynomials. For the results shown in this paper, fourth- to seventh-order polynomials were used, depending on the Reynolds number.

Once the simulation had achieved a periodic state, the velocity field was averaged over a cycle. For the two-dimensional simulations, the velocity field was averaged over time. For the three-dimensional simulations, the spatial spanwise mean was first calculated at each time interval. Because of the use of a Fourier decomposition, this was achieved by simply extracting the zeroth Fourier mode. The temporal mean of these spatial means was then calculated to arrive at the final mean flow. Typically, this was done over about 40 cycles after the asymptotic state was reached, as the three-dimensional flow is only quasi-periodic.

2.2. *Global eigenfrequencies*

The global stability properties of the mean wakes were determined directly, using a standard linear stability analysis. For this analysis, perturbation equations were formed from the linearized incompressible Navier–Stokes equations. The perturbations studied were themselves two-dimensional; no variation along the span of the cylinder was considered, resulting in the equations

$$\frac{\partial \boldsymbol{u}'}{\partial t} = -[(\boldsymbol{u}' \cdot \nabla)\boldsymbol{U} + (\boldsymbol{U} \cdot \nabla)\boldsymbol{u}'] - \nabla P' + Re^{-1}\nabla^2 \boldsymbol{u}', \tag{2.1}$$

$$\nabla \cdot \boldsymbol{u}' = 0, \tag{2.2}$$

where $\boldsymbol{u}'$ is the perturbation velocity field, $\boldsymbol{U}$ is the base flow velocity field and P' is the perturbation pressure field. These equations were solved using the same spectral-element method briefly outlined in § 2.1. The leading global modes were found by considering the equations for the perturbation as an eigenvalue problem:

$$\frac{\partial \boldsymbol{u}'}{\partial t} = \boldsymbol{L}\boldsymbol{u}'. \tag{2.3}$$

The leading eigenmodes and eigenvalues of $\boldsymbol{L}$ were then found using an Arnoldi decomposition, from which the growth rates and frequencies could be determined. The method employed for the Arnoldi decomposition was essentially the same as that described by Tuckerman & Barkley (2000) and Blackburn & Lopez (2003).

2.3. *Global frequency selection from local properties: the saddle-point criterion*

In an effort to relate the local properties of the mean flow to the global behaviour and, in particular, the global frequency selection of the cylinder wake, a saddle-point criterion was employed. The use of a saddle-point criterion for frequency selection analysis was developed for use with quasi-parallel flows that are slowly varying in the flow direction (Le Dizès *et al.* 1996), but has been successfully applied to mean bluff-body wake flows (Hammond & Redekopp 1997; Pier 2002; Thiria & Wesfreid 2007; Khor *et al.* 2008*b*).

In this case, the mean wake flow is treated as a slowly varying parallel flow. This means that streamwise velocity profiles (blatantly ignoring the cross-stream component) can be extracted at a series of x stations down the mean wake, where x denotes the distance downstream from the centre of the cylinder. Because of the assumption that the flow is slowly varying in the x direction, each of the profiles can be treated independently, and a characteristic complex frequency can be found for each.

The characteristic frequency for a given profile is associated with a local group velocity of zero. To find these zeros, a local dispersion relation is required. For the current study, the Rayleigh stability equation, derived from the Euler equations (Drazin & Reid 2004), is used. The equation is

$$(U - c)\left(\frac{\mathrm{d}^2\phi}{\mathrm{d}y^2} - k^2\phi\right) - \frac{\mathrm{d}^2 U}{\mathrm{d}y^2}\phi = 0, \tag{2.4}$$

where U is the base flow profile, c is the complex wave speed and k is the complex wavenumber. The complex frequency is defined as $\omega = kc$.

The zero-group velocity condition is satisfied at 'pinch' points in the complex k plane, which coincide with cusp points in the complex ω plane (Huerre & Rossi 1998). Performing this process for each profile results in complex frequency ω as a function of downstream distance, x. This can be thought of as a global dispersion relation.

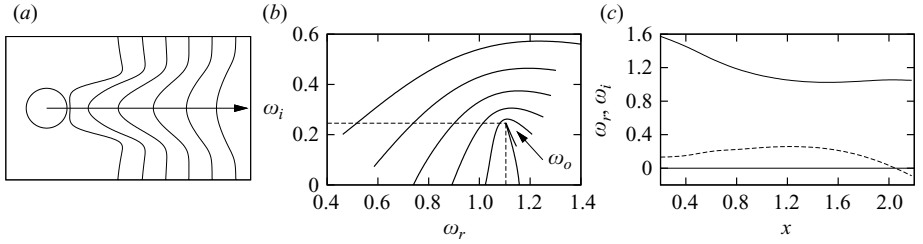

FIGURE 1. The various stages in the procedure of finding the saddle point to find the globally selected frequency from local properties. (*a*) Streamwise velocity profiles are extracted at a series of x stations in the mean wake; (*b*) contours, each relating to a different imaginary value of the wavenumber, are drawn out in the complex ω plane as functions of the real component of the wavenumber until a cusp point is found defining the local characteristic frequency for the given profile; (*c*) the local characteristic frequency as a function of x, which can then be used to find the location of the saddle point in the complex X plane. The solid line represents the real component of frequency, ω_r and the dotted line represents the imaginary component of frequency, ω_i. The data for all these plots are for the mean wake of a circular cylinder at $Re = 100$, and the local profile used to produce (*b*) was that at $x = 1.0$

Here, finding a zero group velocity, or $\partial\omega/\partial X = 0$, will give a characteristic global frequency. This zero group velocity occurs at saddle points in the complex X plane, and they are found by extending $\omega(x)$ off the real axis using analytic continuation and the Cauchy–Riemann equations.

While the mathematics and reasoning behind this analysis can seem quite daunting, in practice it is a relatively mechanical task. The process is as follows:

(i) Compute the mean wake flow;

(ii) From this mean wake, extract profiles of streamwise velocity down the wake, as shown in figure 1(*a*);

(iii) Solve the Rayleigh equation for complex frequencies for purely real wavenumbers for the first profile. This will draw out a contour on the complex ω plane;

(iv) Negatively increment the imaginary component of the wavenumber and again solve the Rayleigh equation for complex frequencies as a function of the real component of the wavenumber, drawing a second contour on the complex ω plane;

(v) Continue this incrementing process until the complex frequency contour drawn produces a cusp. The complex frequency at this cusp is the characteristic frequency for the given profile. An example of the series of contours produced by this process is shown in figure 1(*b*);

(vi) Repeat this process for each profile, building up $\omega(x)$. An example of such a function is shown in figure 1(*c*);

(vii) Find the local minima of the real component of $\omega(x)$;

(viii) Use a truncated Taylor series expansion and the Cauchy–Riemann equations to analytically continue the function into the complex X plane, and locate the saddle point.

This process is referred to as the cusp-map method and is due to Kupfer, Bers & Ram (1987), and it is also well described by Schmid & Henningson (2001).

The technical details of the current study are as follows. Each extracted profile consisted of 512 equispaced points from $y/D = -3$ to $y/D = 3$. For a given value of k, the solution of (2.4) presents an eigenvalue problem in ω. Equation (2.4) was solved over the whole domain by stepping out from one side, employing the boundary

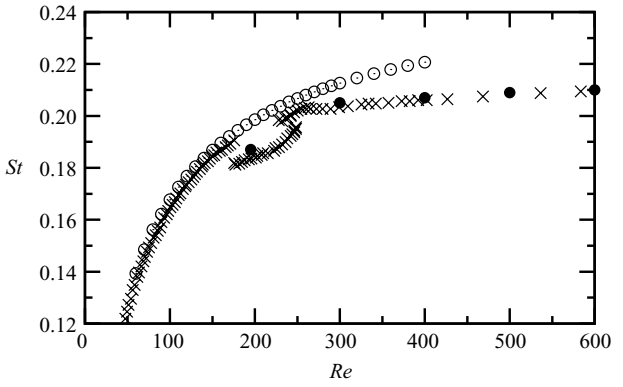

FIGURE 2. Measured simulation frequencies from the two- and three-dimensional simulations compared with the experimental data from Williamson (1989). Here, × represents the data from Williamson (1989); ○ represents the measured frequency from the two-dimensional simulations; ● represents the measured frequency from the three-dimensional simulations. Where the dimension of the simulation matches the physical reality, the measured simulation frequencies are in excellent agreement with the experimental data.

condition at $y = -3$ that $\phi = 0$, justified by the physical fact that $\phi \to 0$ as $y \to \pm\infty$. The stepping was done using a standard fourth-order Runge–Kutta method. The same boundary condition at the other end of the domain, $\phi = 0$ at $y = 3$, was then satisfied using a shooting method, employing a complex Newton method to converge to the correct eigenvalue and therefore ω. Solving over the whole domain in this way, and not imposing any symmetry condition on the perturbation mode ϕ, meant any modes present could be found. In practice, two modes were found for the present profiles: one symmetric and the other antisymmetric, corresponding to the sinuous and varicose modes known to exist in the wakes of circular cylinders (Monkewitz & Nguyen 1987). The sinuous mode is responsible for Kármán-Bénard vortex shedding, and hence this mode was tracked for the results presented in this paper.

2.4. *Validation*

As the primary aim of both the analysis methods presented in this paper was to find the global frequency of a given wake flow, their results are easily validated by comparing with the measured frequency from the simulation that produced the base flow. These measured frequencies are compared with existing data in figure 2. Here, the measured frequencies are compared with the experimental data from Williamson (1989).

The figure shows that for $Re < 180$, below the first transition to three-dimensional flow, the measured frequencies from the two-dimensional simulations are in excellent agreement with the experimental data. For $Re > 180$, the measured two-dimensional simulation frequencies diverge from the experimental measurements, as three-dimensional effects become more important. However, the results are in excellent agreement with two-dimensional simulations from other studies (Barkley & Henderson 1996; Henderson 1997).

The measured frequencies from the three-dimensional simulations show no such divergence and follow the experimental measurements very closely over all Reynolds numbers, including those in the discontinuous region of the Strouhal curve, when $180 \leqslant Re \leqslant 250$. These results provide a high level of confidence that the simulations are adequately resolved in space and time to faithfully capture all of the relevant

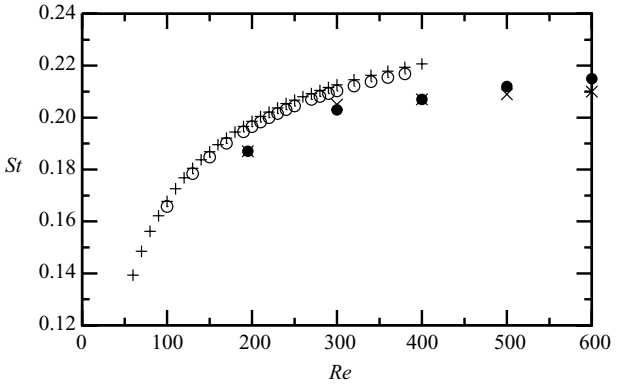

FIGURE 3. Global eigenfrequencies from analysis of the mean flow, compared with directly measured frequencies from the simulations. Here, + indicates the directly measured frequency from the two-dimensional simulations; × indicates the directly measured frequency from the three-dimensional simulations; ○ indicates the global eigenfrequency from the two-dimensional simulations; ● indicates the global eigenfrequency from the three-dimensional simulations. In all cases, the global eigenfrequency closely matches the directly measured frequency.

physics of the problem. Because of this, the global frequencies calculated using both the local profiles and the global stability analysis are compared with the frequencies directly measured from the present simulations throughout the rest of the paper.

3. Results

3.1. *Global stability analysis*

The frequency of the leading global mode growing on the mean cylinder wake (referred to as the eigenfrequency) as a function of Reynolds number is presented in figure 3. The match between the eigenfrequencies and the measured frequencies is very close, for both the mean wakes of the two-dimensional and three-dimensional simulations. Note that the match occurs for both the modes A and B (Williamson 1988) shedding regimes. The results from the two-dimensional simulations effectively extend the parameter range of the study of Barkley (2006).

For all the cases tested, the magnitudes of the eigenvalues associated with the leading global mode were close to unity, suggesting that the mean wake flow is marginally stable.

While similar findings have been previously reported for the mean cylinder wake at relatively low Reynolds numbers by Barkley (2006), this is the first time that such a finding has been reported over such an extended range of Re, and certainly the first time that this result has been reported for the mean wake of the three-dimensional flow. This result could not obviously be extracted from the lower-Re results. The asymptotic analysis of Sipp & Lebedev (2007) showed that the eigenfrequency of the leading global mode growing on the mean wake closely matched the saturated global frequency when the level of nonlinear interaction between the mean and the first global mode is relatively low. The results of this study indicate that this condition is still met when the cylinder wake is three-dimensional.

Representations of the leading global modes are shown in figures 4 and 5. These images present the perturbation vorticity. The images show that the spatial wavelength of the leading global mode in the streamwise direction is similar to that of the eventual saturated Kármán–Bénard vortex street. For example, the spatial wavelength was

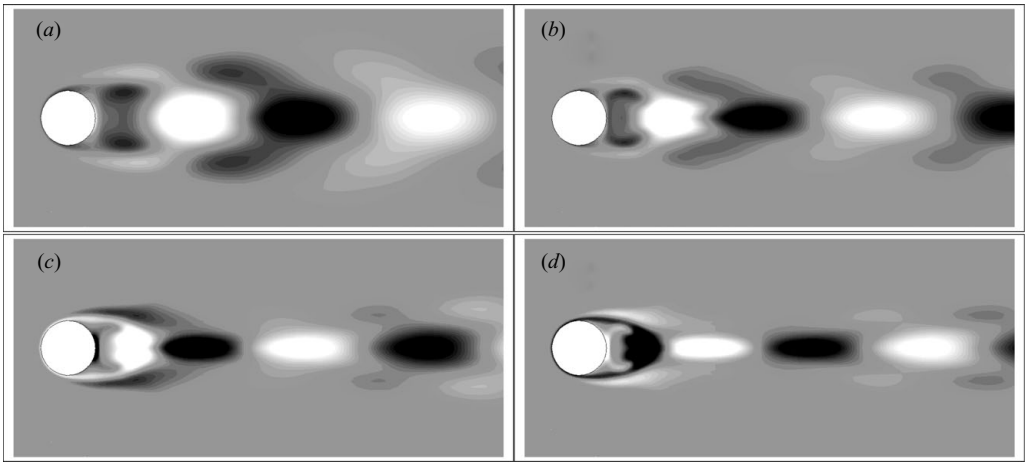

FIGURE 4. The leading global mode from the two-dimensional simulations. Black (white) contours represent negative (positive) perturbation vorticity. (*a*) $Re = 100$; (*b*) $Re = 200$; (*c*) $Re = 300$; (*d*) $Re = 400$. With increasing Re, the global mode becomes more highly concentrated along the wake centreline, reflecting the narrowing of the mean wake.

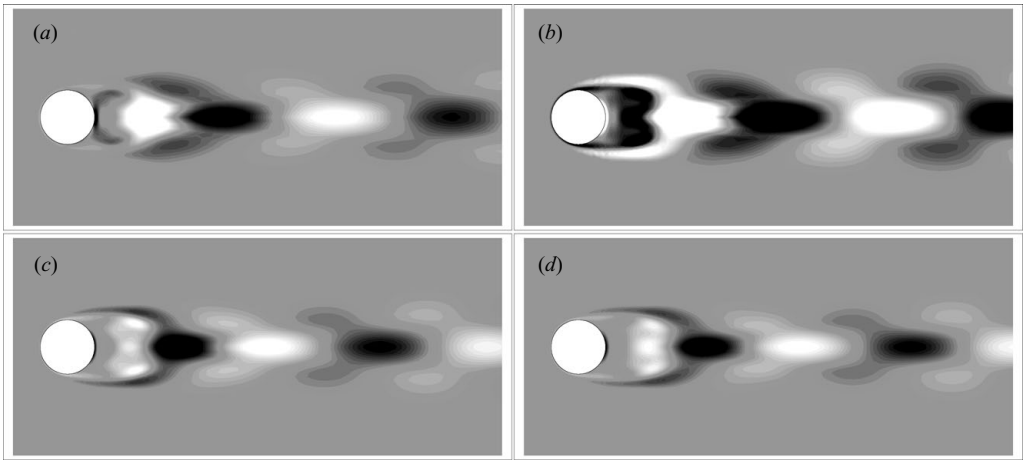

FIGURE 5. The leading global mode from the three-dimensional simulations. Black (white) contours represent negative (positive) perturbation vorticity. (*a*) $Re = 300$; (*b*) $Re = 400$; (*c*) $Re = 500$; (*d*) $Re = 600$.

estimated by measuring the distance between the points on the wake centreline where the transverse velocity crossed zero. Doing this for the fully saturated flow and the global mode at $Re = 100$ produced a maximum difference of around 10 % in the estimate of the spatial wavelength. With increasing Re, the global modes become more highly concentrated on the wake centreline, reflecting the narrowing of the wake with increasing Re.

Comparing figures 4(*c*) and 4(*d*) with 5(*a*) and 5(*b*) shows the direct influence of the three-dimensionality on the leading two-dimensional global mode growing on the mean wake at $Re = 300$ and $Re = 400$, respectively. The main effect of three-dimensionality is to increase the width of the global mode, reflecting the increased

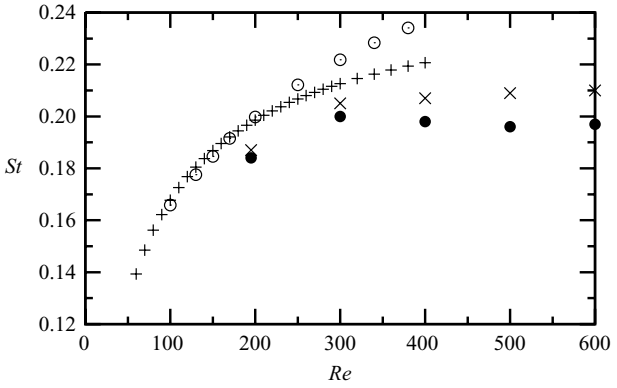

FIGURE 6. Saddle-point frequencies from analysis of the mean flow, compared to directly measured frequencies from the simulations. Here, + indicates the directly measured frequency from the two-dimensional simulations; × indicates the directly measured frequency from the three-dimensional simulations; ○ indicates the saddle-point frequency from the two-dimensional simulations; ● indicates the saddle-point frequency from the three-dimensional simulations. The divergence of the saddle-point frequency from the two-dimensional simulations from the measured frequency for $Re > 250$ is attributed to the shortening recirculation length.

width of the mean wake. The general structure of the global mode is essentially unaffected by the presence of three-dimensionality.

3.2. *Local stability analysis*

Figure 6 presents the frequencies calculated from the saddle-point criterion, for the mean wakes from both the two- and three-dimensional simulations. Focusing first on the results from the two-dimensional simulations, there are a number of features that justify some explanation. First, the match between the measured frequency and the saddle-point frequency is very close for $Re < 200$. This is despite the fact that the local stability analysis was based on solving the Rayleigh stability equation, which ignores all viscous damping of the perturbation. Interestingly, Pier (2002) conducted the same analysis over the Reynolds number range $Re < 200$ using the viscous Orr–Sommerfeld equation and found that the frequencies at the saddle point were slightly underpredicted.

For higher Re, the match between the saddle-point frequency and the measured frequency is not as close, and the two continue to diverge with increasing Re. At first, this appears to be counterintuitive, as it would be expected that an inviscid analysis would become more accurate with increasing Re. However, the current analysis relies on the fundamental assumption that the base flow is parallel and slowly varying in the x direction, and it is this assumption that is broken at higher Re for the two-dimensional simulations.

Figure 7 presents the mean base flow vorticity from the two-dimensional simulations over $100 \leqslant Re \leqslant 400$. This series of images clearly shows that with increasing Re, the recirculation length significantly shortens. The recirculation length is the length over which there is reversed flow on the wake centreline. It therefore represents the end of the forming vortex pair in the wake. As this length becomes shorter, the local curvature of the flow in this region becomes higher, and the flow evolves significantly over a short distance, thereby violating the primary assumption of the analysis. It

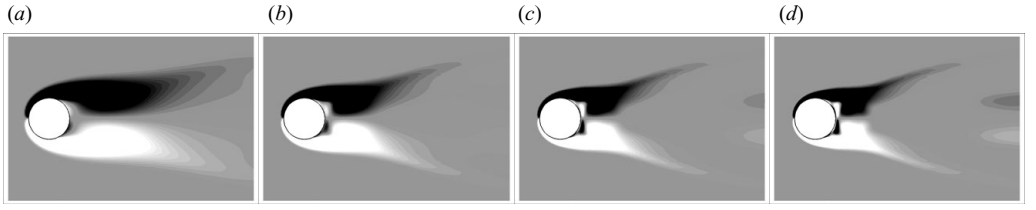

FIGURE 7. Mean wakes from the two-dimensional simulations. Black (white) contours represent negative (positive) vorticity. (*a*) $Re = 100$; (*b*) $Re = 200$; (*c*) $Re = 300$; (*d*) $Re = 400$. With increasing Re, the mean wake becomes narrower and the recirculation length (mirrored by the length of the vortices in the near wake) becomes shorter.

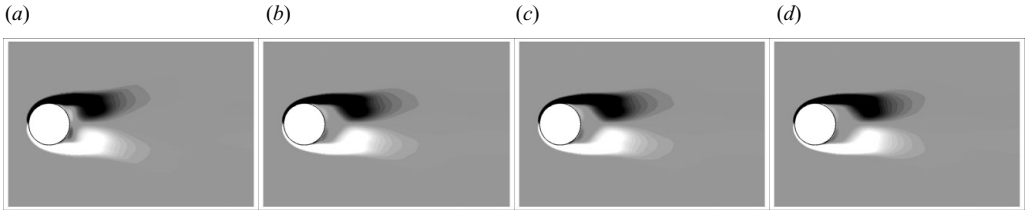

FIGURE 8. Mean wakes from the three-dimensional simulations. Black (white) contours represent negative (positive) vorticity. (*a*) $Re = 300$; (*b*) $Re = 400$; (*c*) $Re = 500$; (*d*) $Re = 600$. Opposite to the two-dimensional results, the recirculation length (mirrored by the length of the vortices in the near wake) actually increases slightly with increasing Re.

is for this region that the saddle-point analysis is not able to accurately recover the global frequency for $Re \geqslant 250$ for the two-dimensional simulations.

Turning to the results from the three-dimensional simulations, the saddle-point analysis does a surprisingly good job of recovering the global frequency over the range $195 \leqslant Re \leqslant 600$, as shown in figure 6. This is particularly true for $195 \leqslant Re \leqslant 400$, where the saddle-point frequency from the three-dimensional mean wake is closer to the measured simulation frequency than its two-dimensional counterpart. Again, this appears to be a consequence of the local curvature and the rate of variation with downstream distance. Figure 8 shows the mean wake vorticity from the three-dimensional simulations. This series of images shows that the recirculation region does not shorten with increasing Re (at least for $Re \geqslant 250$) when the flow is three-dimensional. Also, comparing figures 7(*c*) and 7(*d*) ($Re = 300$ and $Re = 400$ from the two-dimensional simulations) with figures 8(*a*) and 8(*b*) ($Re = 300$ and $Re = 400$ from the three-dimensional simulations) directly shows the impact of the flow becoming three-dimensional. The recirculation for the three-dimensional cases is clearly longer, meaning that the assumptions for the saddle-point analysis are closer to reality, explaining the success of the analysis over this range of Re.

The recirculation length results are summarized in figure 9, where the recirculation lengths from both the two- and three-dimensional simulations are plotted as a function of Re. The recirculation length was defined as the length where the mean streamwise velocity crossed from negative to positive on the wake centreline. Also plotted in this figure is the downstream distance to the real location of the saddle point. Also, to show that the saddle points do indeed lie near the real axis, the imaginary coordinates of the saddle points are shown.

The shortening of the recirculation length with increasing Re for the two-dimensional simulations is clearly evident. It is also shown that this trend is reversed

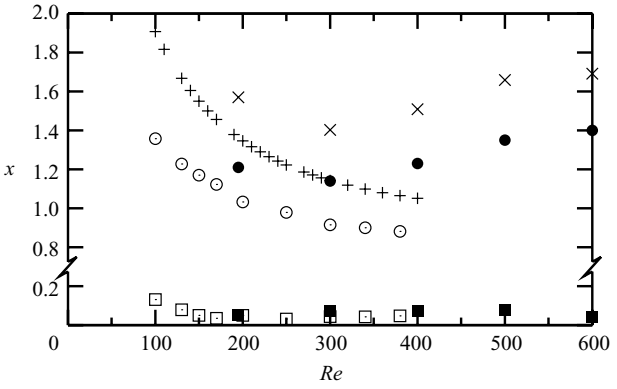

FIGURE 9. Recirculation lengths and saddle-point positions from the two- and three-dimensional simulations. Here, + represents the recirculation length measured from the two-dimensional simulations; × represents the recirculation length measured from the three-dimensional simulations; ○ represents the real coordinate of the saddle-point location from the two-dimensional simulations; ● represents the real coordinate of the saddle-point location from the three-dimensional simulations; □ represents the imaginary coordinate of the saddle-point location from the two-dimensional simulations; ■ represents the imaginary component of the saddle-point location from the three-dimensional simulations.

when the flow is three-dimensional. Figure 9 also shows that the distance to the saddle point (the real coordinate of the saddle point) correlates with the recirculation length. While no definitive relation is offered for this, an inspection of the mean wake plots of figures 7 and 8 shows that the saddle point occurs in a region of the flow where the mean flow is closest to parallel. This is consistent with the theory, as the saddle point occurs when $\partial\omega/\partial X = 0$. In regions where the mean flow is locally close to parallel, it is also relatively slowly varying, and hence the local characteristic values of ω for successive profiles will be quite similar and $\partial\omega/\partial X \to 0$.

As an aside, note that for all the mean flows investigated, none of them had a transition from convective to absolute instability in a region of the flow beyond the base of the cylinder (i.e. beyond $x = 0.5D$). Note that all of the results for this study were obtained tracking the symmetric sinuous mode, which by definition is largest on the wake centreline. For profiles where $x < 0.5$, this centreline is actually inside the cylinder body. It is therefore not simple to interpret what mode growth in this region means, and so no other frequency selection criteria such as the initial resonance condition (Pier & Huerre 2001) were tested.

4. Concluding remarks

Both global and local stability analyses have been conducted for the cylinder wake, based on both two- and three-dimensional simulations, for $Re \leqslant 600$. In all cases, the temporal (and for the three-dimensional case, the spanwise-averaged) mean flow was analysed.

The global analysis showed that for both the two- and three-dimensional flows, the mean wake remains close to marginally stable and that the eigenfrequency of the leading global mode is very close to the saturated frequency measured from the direct numerical simulation, the difference being within 2.5 % over the entire range tested. Hence, even for the fully three-dimensional flow (at least up to $Re = 600$), the nonlinear corrected base flow appears to take the role of a new base state for

linear modes to grow on, with little nonlinear interaction between the mean and the leading global mode (Sipp & Lebedev 2007; Thiria & Wesfreid 2007). This behaviour appears to persist far from the bifurcation point. This result builds upon that of Barkley (2006).

For the local analysis, a saddle-point criterion has been applied, based on a slowly varying, locally parallel set of assumptions. When the base flow was two-dimensional, the global frequency recovered from this analysis matched the measured simulation frequency very closely for $Re < 250$, confirming the findings of Pier (2002). However, at higher values of Re, the saddle-point frequency diverged from the measured frequency, probably due to the shortening recirculation length increasing the local curvature and rate of variation, thereby breaking the underlying assumptions of the analysis. For the three-dimensional flow, the saddle-point frequency reasonably predicted the measured frequency because of an increase in recirculation length, rendering the analysis valid.

The reasonable success of the local analysis up to $Re = 600$ and the very good prediction of the global frequency from the global analysis indicate that, even when fully three-dimensional, the cylinder wake dynamics are dominated by the first linear mode growing on a nonlinear corrected mean flow.

The authors acknowledge the support of the National Computational Infrastructure National Facility through the Merit Allocation Scheme (grant N67) for the provision of the computational resources used for the simulations of this study. The authors also acknowledge the financial support of the Australian Research Council through the Discovery Grants program (grants DP0877327, DP0878304 and LX0668992).

REFERENCES

Barkley, D. 2006 Linear analysis of the cylinder wake mean flow. *Europhys. Lett.* **75** (5), 750–756.

Barkley, D. & Henderson, R. D. 1996 Three-dimensional Floquet stability analysis of the wake of a circular cylinder. *J. Fluid Mech.* **322**, 215–241.

Blackburn, H. M. & Lopez, J. M. 2003 On three-dimensional quasi-periodic Floquet instabilities of two-dimensional bluff body wakes. *Phys. Fluids* **15**, L57–L60.

Chomaz, J. M. 2005 Global instabilities in spatially developing flows: non-normality and nonlinearity. *Annu. Rev. Fluid Mech.* **37**, 357–392.

Drazin, P. G. & Reid, W. H. 2004 *Hydrodynamic Stability*, 2nd edn. Cambridge University Press.

Hammond, D. & Redekopp, L. 1997 Global dynamics of symmetric and asymmetric wakes. *J. Fluid Mech.* **331**, 231–260.

Henderson, R. 1997 Nonlinear dynamics and pattern formation in turbulent wake transition. *J. Fluid Mech.* **352**, 65–112.

Huerre, P. & Monkewitz, P. A. 1985 Absolute and convective instabilities in free shear layers. *J. Fluid Mech.* **159**, 151–168.

Huerre, P. & Rossi, M. 1998 Hydrodynamic instabilities in open flows. In *Hydrodynamics and Nonlinear Instabilities* (ed. C. Godrèche & P. Manneville), pp. 81–294. Cambridge University Press.

Khor, M., Sheridan, J. & Hourigan, K. 2008*a* The response of the shear layer separating from a circular cylinder to acoustic perturbation. *J. Fluid Mech.* **601**, 425–441.

Khor, M., Sheridan, J., Thompson, M. C. & Hourigan, K. 2008*b* Global frequency selection in the observed time-mean wakes of circular cylinders. *J. Fluid Mech.* **601**, 425–441.

Kupfer, K., Bers, A. & Ram, A. K. 1987 The cusp map in the complex-frequency plane for absolute instabilities. *Phys. Fluids* **30** (10), 3075–3082.

Le Dizès, S., Huerre, P., Chomaz, J. M. & Monkewitz, P. A. 1996 Linear global modes in spatially developing media. *Phil. Trans. Roy. Soc. Lond.* **354**, 169–212.

Leontini, J. S., Thompson, M. C. & Hourigan, K. 2007 Three-dimensional transition in the wake of a transversely oscillating cylinder. *J. Fluid Mech.* **577**, 79–104.

Monkewitz, P. A. & Nguyen, L. N. 1987 Absolute instabilities in the near-wake of two-dimensional bluff bodies. *J. Fluids Struct.* **1**, 165–184.

Pier, B. 2002 On the frequency selection of finite-amplitude vortex shedding in the cylinder wake. *J. Fluid Mech.* **458**, 407–417.

Pier, B. & Huerre, P. 2001 Nonlinear self-sustained structures and fronts in spatially developing wake flows. *J. Fluid Mech.* **435**, 145–174.

Ryan, K., Thompson, M. C. & Hourigan, K. 2005 Three-dimensional transition in the wake of elongated bluff bodies. *J. Fluid Mech.* **538**, 1–29.

Schmid, P. & Henningson, D. S. 2001 *Stability and Transition in Shear Flows*. Springer.

Sipp, D. & Lebedev, A. 2007 Global stability of base and mean flows: a general approach and its applications to cylinder and open cavity flows. *J. Fluid Mech.* **593**, 333–358.

Thiria, B. & Wesfreid, J. E. 2007 Stability properties of forced wakes. *J. Fluid Mech.* **579**, 137–161.

Thompson, M. C., Hourigan, K. & Sheridan, J. 1996 Three-dimensional instabilities in the wake of a circular cylinder. *Exper. Thermal Fluid Sci.* **12**, 190–196.

Thompson, M. C., Leweke, T. & Williamson, C. H. K. 2001 The physical mechanism of transition in bluff body wakes. *J. Fluids Struct.* **15**, 607–616.

Tuckerman, L. S. & Barkley, D. 2000 *Numerical Methods for Bifurcation Problems and Large-scale Dynamical Systems* (chap. Bifurcation analysis for timesteppers), pp. 453–566. Springer.

Williamson, C. H. K. 1988 The existence of two stages in the transition to three dimensionality of a cylinder wake. *Phys. Fluids* **31**, 3165–3168.

Williamson, C. H. K. 1989 Oblique and parallel modes of vortex shedding in the wake of a circular cylinder at low Reynolds numbers. *J. Fluid Mech.* **206**, 579–627.